The DNA Binding Activity of p53 Displays Reaction-Diffusion Kinetics

Peter Hinow,* Carl E. Rogers,† Christopher E. Barbieri,‡ Jennifer A. Pietenpol,‡ Anne K. Kenworthy,† and Emmanuele DiBenedetto*

*Department of Mathematics, Vanderbilt University, Nashville, Tennessee; †Department of Molecular Physiology and Biophysics, Vanderbilt University School of Medicine, Nashville, Tennessee; and ‡Department of Biochemistry, Center in Molecular Toxicology, Vanderbilt-Ingram Cancer Center, Vanderbilt University Medical Center, Nashville, Tennessee

ABSTRACT The tumor suppressor protein p53 plays a key role in maintaining the genomic stability of mammalian cells and preventing malignant transformation. In this study, we investigated the intracellular diffusion of a p53-GFP fusion protein using confocal fluorescence recovery after photobleaching. We show that the diffusion of p53-GFP within the nucleus is well described by a mathematical model for diffusion of particles that bind temporarily to a spatially homogeneous immobile structure with binding and release rates k_1 and k_2, respectively. The diffusion constant of p53-GFP was estimated to be $D_{\text{p53-GFP}} = 15.4\ \mu\text{m}^2\,\text{s}^{-1}$, significantly slower than that of GFP alone, $D_{\text{GFP}} = 41.6\ \mu\text{m}^2\,\text{s}^{-1}$. The reaction rates of the binding and unbinding of p53-GFP were estimated as $k_1 = 0.3\ \text{s}^{-1}$ and $k_2 = 0.4\ \text{s}^{-1}$, respectively, values suggestive of nonspecific binding. Consistent with this finding, the diffusional mobilities of tumor-derived sequence-specific DNA binding mutants of p53 were indistinguishable from that of the wild-type protein. These data are consistent with a model in which, under steady-state conditions, p53 is latent and continuously scans DNA, requiring activation for sequence-specific DNA binding.

INTRODUCTION

A valuable tool to probe the architecture of the cell nucleus is fluorescence recovery after photobleaching (FRAP) (reviewed in 1–5). FRAP studies have revealed that many proteins involved in nuclear processes are highly mobile, yet diffuse more slowly than nonreactive, inert proteins of comparable size (such as green fluorescent protein, GFP) in vivo (6–8). Careful analysis shows that for some of these proteins, FRAP recovery curves exhibit biphasic behavior, with a fast initial diffusion-dominated phase followed by a slow, reaction-dominated turnover phase (9). Such behavior is characteristic of the binding and unbinding of fluorescently-labeled molecules to an immobile structure (immobile on the timescale of the experiment); decreasing the effective diffusion constant of the protein is observed. This behavior can be described by a mathematical model (7,9,10) based on a reaction-diffusion equation for a mobile and an immobile species that interact through first-order chemical reactions. Such a model and a related compartmental model have been used by Carrero et al. (11) to study the diffusion and binding behavior of nuclear actin and the chromatin-associated histone H1. Similar behavior has also been observed in studies by Sprague et al. (7) of the diffusional mobility of the transcription factor glucocorticoid receptor, GFP-GR.

Analytical solutions for the reaction-diffusion model have been derived for both circular and rectangular bleach geometries (7,10). For the latter case, the model assumes that the spatial domain available for diffusion of the fluorescent molecule of interest is a rectangle with one of its sides identified with the interval $(0, \ell)$. The density of the fluorescent molecules is assumed to be independent of the longitudinal variable of the rectangle and thus is a function $u(x, t)$ of $x \in (0, \ell)$ and time t (10). The mathematical model is based on a reaction-diffusion equation for the density $u(x, t)$ set in the interval $(0, \ell)$ for all times $t > 0$, starting from its initial datum u_0. The remaining boundary conditions on $x = 0$ and $x = \ell$ are of zero flux, since the fluorescent molecules are not permitted to outflow their compartment. The parameters at play are the diffusion coefficient D, and the binding rate k_1 to an immobile structure, and the release rate k_2 from it. The values $k_1 = k_2 = 0$ would correspond to absence of immobile binding structures and thus free diffusion for $u(x, t)$. The density of fluorescent molecules $u(x, t)$ is integrated over a subinterval of $(0, \ell)$, called region of interest (ROI), and generates a theoretical, time-dependent, fluorescence signal $F(t; D, k_1, k_2)$, depending upon the unknown diffusion parameters $\{D, k_1, k_2\}$. By fitting the theoretical function to the experimental data, one obtains estimates for these parameters.

Motivated by the key role of p53 in cancer biology and its well-characterized biochemistry, we determined whether the diffusional mobility of p53 within the nucleus can be described by the reaction-diffusion model. The tumor suppressor p53 is the most commonly mutated gene in human cancer. In response to cell stress, such as oncogene activation or DNA damage, p53 can function as a sequence-specific DNA binding transcription factor. p53 activates the transcription of genes involved in the processes of cell cycle arrest, DNA repair, and apoptosis, thereby protecting the genome from mutations and the organism as a whole from tumor formation.

Submitted November 22, 2005, and accepted for publication March 3, 2006.

Peter Hinow and Carl E. Rogers contributed equally to this study.

Address reprint requests to Anne K. Kenworthy, Tel.: 615-322-6615; E-mail: anne.kenworthy@vanderbilt.edu, or Emmanuele DiBenedetto, Tel.: 615-343-5906; E-mail: em.diben@vanderbilt.edu.

0006-3495/06/07/330/13 $2.00

doi: 10.1529/biophysj.105.078303

Although there have been numerous studies analyzing p53 binding to DNA using in vitro assays (reviewed in (12)), few studies have reported on the analysis of p53 interaction with DNA in an intact cell. Using confocal FRAP, we analyzed the lateral diffusion of a GFP-tagged form of p53. We extended the reaction-diffusion model to allow for flexibility in choosing the initial data by distinguishing the region where the bleaching laser beam is concentrated from the initial distribution profile of fluorescent molecules. This permits one to take into account the diffusion of unbleached molecules into the bleach spot and the diffusion of bleached molecules out of the bleach spot during the application of the bleaching laser beam, factors that can otherwise lead to an erroneous estimation of diffusion constants from confocal FRAP measurements (13,14). In addition, we used a nested model approach to test the statistical significance of fitting the data using the reaction-diffusion model versus simple free diffusion.

We observed a significant difference in the diffusive behavior of p53-GFP compared to GFP alone. Whereas the recovery data of GFP can be fit satisfactorily with a one-parameter model involving only free diffusion, the recovery of p53-GFP is well described by a reaction-diffusion model with three parameters, the diffusion constant D, and k_1 and k_2, which are the binding and release rates of the diffusing species to an immobile structure, respectively. Our mathematical and statistical interpretations of the data suggest that p53-GFP binds to, and is released from, an immobile structure. This binding event is transient, as our data ruled out the existence of an immobile fraction. An alternative model that incorporates fluorescent molecules of different mobilities could be ruled out on physical grounds, as it would have predicted a fraction of p53-GFP diffuses faster than GFP alone. We further showed that the diffusional mobility of tumor-derived mutants of p53 that are unable to bind DNA in a sequence-specific manner is similar to that of wild-type p53-GFP. These data indicate p53 predominantly undergoes nonspecific DNA binding under steady-state conditions. The results are consistent with previous in vitro studies showing that p53 is latent until activated by another number of conditions including genotoxic stress (15). We also found that the diffusion coefficient of unbound p53-GFP is significantly slower than that of GFP alone, likely reflecting the presence of p53 oligomers.

MATERIALS AND METHODS

Cell culture and treatment

H1299 human large cell lung carcinoma cells were cultured in Dulbecco-modified Eagle medium (Gibco BRL, Gaithersburg, MD) supplemented with 10% fetal calf serum and 1% penicillin-streptomycin. All cells were cultured at 37°C with 5% CO_2.

Plasmids and cell transfection

Wild-type p53 and tumor-derived mutants p53-R175H and p53-R273H were subcloned into the pEGFP-N1 plasmid (Promega, Fitchburg, WI) in-frame with EGFP using the *Xho*I and *Pst*I restriction sites. H1299 cells, which are deficient for p53, were transfected using Fugene 6 (Roche, Indianapolis, IN) according to the manufacturer's protocols. Twenty-four hours after transfection, cells were analyzed by confocal fluorescent microscopy or harvested for protein analysis as described below.

Protein lysate preparation and Western analysis

Trypsinized cells were washed with ice-cold PBS, and lysed in kinase lysis buffer (50 mM Tris-HCl (pH 7.4), 150 mM NaCl, 0.1% Nonidet P-40 (AppliChem, Darmstadt, Germany), 0.1% Triton X-100 (Sigma-Aldrich, St. Louis, MO), 4 mM EDTA, and 1 mM dithiothreitol containing the phosphatase inhibitors 50 mM NaF, 0.2 mM sodium vanadate, 10 mM *p*-nitrophenyl phosphate, and 10 mM β-glycerophosphate and the protease inhibitors antipain (10 μg/ml), leupeptin (10 μg/ml), pepstatin A (10 μg/ml), chymostatin (10 μg/ml; Sigma-Aldrich), and 4-(2-aminoethyl)-benzenesulfonyl-fluoride (200 μg/ml; Calbiochem, San Diego, CA). Cells were incubated on ice 45 min, and the protein supernatant was clarified by centrifugation at 13,000 $\times$ g for 10 min at 4°C. Protein concentration was determined by the Bio-Rad protein quantification kit (Bio-Rad Laboratories, Hercules, CA). Western analysis was performed as previously described in Flatt et al. (16) with the following primary antibodies: α-p53 monoclonal antibody 1801 (Oncogene Research Products, Calbiochem, Boston, MA), α-WAF1 monoclonal antibody Ab-1 (Oncogene), and α-β-actin polyclonal antibody I-19 (Santa Cruz Biotechnology, Santa Cruz, CA). Uniformity of protein loading was assessed by β-actin analyses, as well as by fast green staining of the membranes. A Fluor-S Max MultiImager (Bio-Rad) was used to quantify Western signals.

Photobleaching experiments

Fluorescence recovery after photobleaching experiments were performed at 22°C using a Zeiss LSM 510 confocal microscope (Carl Zeiss, Thornwood, NY) with a 40×/1.3 NA Plan-Neofluar objective (17,18). For imaging, cells grown on coverslips were mounted in Dulbecco-modified Eagle medium (Vanderbilt DRTC Diabetes Research and Training Core), supplemented with 25 mM HEPES buffer (Sigma), and 1 mg/ml bovine serum albumin (Sigma) after being washed twice. GFP fluorescence was excited at 488 nm using 1% transmission and emission collected using a 505-nm filter provided by the manufacturer. An image of the whole cell was obtained before and after the experiment. FRAP measurements were performed using a 2.2-μm wide region of interest (ROI 1) centered on the nucleus. Only the ROI was imaged during the measurement. Photobleaching was performed at 100% transmission by scanning the bleach ROI for 10–50 iterations, yielding bleach times of 529 ms and 1010 ms, respectively. Recoveries were collected over 20 s at 79-ms intervals. Fluorescence intensity data for the bleach ROI were calculated using the Zeiss LSM software. The fluorescence time series were exported to ASCII files and are available upon request. FRAP experiments were performed on 3–5 separate days, typically including between 5 and 10 cells per protein on a given day.

The parameters needed for both mathematical models introduced in Mathematical Modeling are the length ℓ of the compartment, the center c of the bleach strip, the half-width of the initial datum h, the half-width of the observation strip r (the region of interest), and the bleach depth θ (Fig. 1). The parameters ℓ and c were determined from pictures taken of each cell before the bleach experiment. For the p53-GFP loaded nuclei, ℓ was estimated in the range between 18 and 24 μm. The ROI was drawn by hand across the entire width of the fluorescent compartment after the fluorescence data had been collected. The region of control (ROC) depicted in Fig. 1 is where fluorescence background intensity is measured as control.

With perhaps improper, but suggestive symbolism, we denote by $ROI(t)$ and $ROC(t)$ the fluorescence measured at time t, in the region of interest ROI and the control region ROC, respectively. The prebleach intensity F_{pre} was taken to be the average of the 20 reduced signal data points collected before the bleach. Thus, the observed, normalized fluorescence is given by

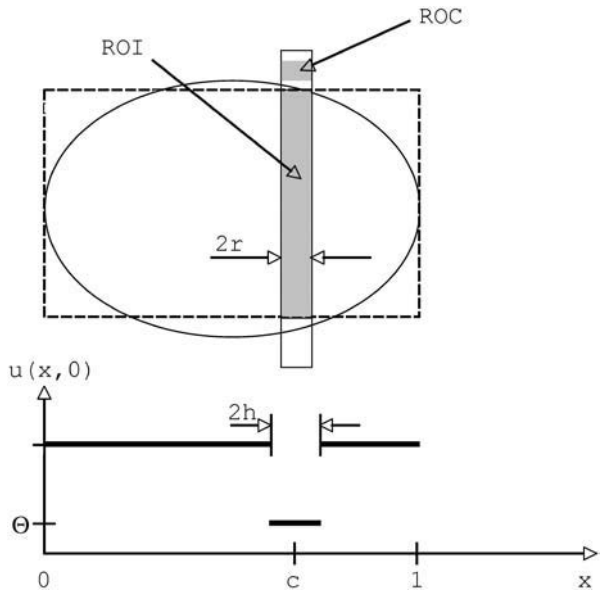

FIGURE 1 The geometrical setup of the experiment. The compartment available to the fluorescent molecules (*solid ellipse*) is approximated by the dashed rectangle, which, in turn, is projected onto its long side of length ℓ. The scanned bleach strip is indicated by the solid rectangle. It is centered at c and has half-width r. The region of interest (ROI) and the region of control (ROC) from which the signal and the background signal, respectively, are collected are shaded gray. The initial datum to the recovery process is piecewise constant, with θ the bleach depth and h the half-width of the bleached region.

$$F_{\text{obs}}(t_i) = \frac{ROI(t_i) - ROC(t_i)}{F_{\text{pre}}}.$$

This normalization is commonly known as ''single'' normalization in the literature (19). The bleach depth θ was taken to be the smallest value of the normalized fluorescence time series, i.e., at the instant when recovery starts. Typically, $\theta = 0.3$ was observed. The ultimate (asymptotic) level of recovery $F_{\infty,\,\text{obs}}$ was taken to be the average of the last five entries of the time series $F_{\text{obs}}(t_i)$. It varied in the range 0.7–0.8.

Analysis of fluorescence recovery data

Fitting the theoretical recovery functions to the experimental recovery curves (see Mathematical Modeling) was done with the MatLab standard function *lsqcurvefit* (Ver. 6.5, The MathWorks, Natick, MA). The series expansions for the recovery derived below were calculated up to 500 terms in all cases. The programs ran on a Dell 4600 computer with dual 2.2 GHz Xeon processors running Linux (Red Hat 7.3, Raleigh, NC). The MatLab codes will be available at http://math.vanderbilt.edu/~hinowp. The statistical significance of the binding rate constant k_1 was determined by the method of Banks and Fitzpatrick (20).

MATHEMATICAL MODELING

General considerations

We will employ two mathematical models for the recovery process. The first is based on free diffusion of a single species and will contain one parameter, the diffusion constant D (21). The second accounts for temporary binding of fluorescent molecules to an immobile structure (7,9–11). It contains three parameters, the (free) diffusion constant D as well as rate constants for the binding and unbinding reaction, k_1 and k_2, respectively. We will extend these models by choosing a more flexible initial condition that allows us to factor in the effects of diffusion in and out of the bleach spot during the bleach time.

We assume a strip bleach geometry (Fig. 1). The diffusion compartment is approximated to be a rectangle of width ℓ, and the concentration $u(x, t)$ of the fluorescent molecules is assumed to be independent of the longitudinal variable on the rectangle. The bleached region is a strip that spans the full width of the rectangle. The mathematical spatial domain thus becomes the interval $[0, \ell]$. Homogeneous Neumann conditions (zero flux condition) are imposed on $u(x, t)$, at the extremities 0 and ℓ. This means no exchange takes place across the boundary of the compartment (the nuclear membrane respective to the plasma membrane). The observation region is the interval centered at c and has length $2r$, modeled by

$$I(x) = \begin{cases} 1 & \text{if } |x-c| \le r \\ 0 & \text{otherwise} \end{cases} \quad x \in [0, \ell]. \tag{1}$$

The model for free diffusion

Let $u(x, t)$ denote the concentration of fluorescent molecules at position x at time t. Such a concentration is normalized to be ''1'' in the steady state of the prebleach phase. The differential equation, boundary condition, and initial condition for u are

$$\frac{\partial}{\partial t}u(x,t) = D\frac{\partial^2}{\partial x^2}u(x,t) \quad x \in (0,\ell), t \ge 0, \tag{2}$$

$$\frac{\partial}{\partial x}u(0,t) = \frac{\partial}{\partial x}u(\ell,t) = 0 \quad t \ge 0, \tag{3}$$

$$u(x,0) = \begin{cases} 1 & \text{if } |x-c| > h \\ \theta & \text{if } |x-c| \le h \end{cases}. \tag{4}$$

Here, c is the center of the bleached region, $2h$ is its width, and $0 \le \theta < 1$ is the bleach depth. Notice the different meaning of r and h and that $r < h$ is possible (Fig. 1). To the best of our knowledge in the current literature, piecewise constant initial profiles are considered with $r = h$ and $\theta = 0$ (7,9,10). Thus, no distinction is made, in particular, between initial datum and observation region at completion of the bleaching process.

A potential limitation of confocal FRAP measurements is that the bleach is accomplished by scanning the laser across the bleach region of interest, a process that takes a finite amount of time. As a result, during the bleach time, unbleached molecules diffuse into the bleach spot, and bleached molecules diffuse out of it (13,14,22). This results in an uncertainty about the initial datum of the recovery process. As remarked by Weiss, the width of the bleached spot is larger

and its boundaries are less sharp. This may cause an underestimation of the diffusion constants by a factor of 2–4 (13).

The greater flexibility in the choice of the initial datum permits one to account for diffusion of fluorescent molecules into the bleach strip during the bleach time. The total mass of the initial datum from Eq. 4 (respectively the total mass of the sum of Eqs. 10 and 11) should match its observed ultimate (asymptotic) recovery value, i.e.,

$$\int_0^\ell u(x,0)\mathrm{d}x = \ell - 2h + 2h\theta = F_{\infty,\mathrm{obs}}\ell. \tag{5}$$

Thus, h must be chosen as

$$h = \frac{\ell(1 - F_{\infty,\mathrm{obs}})}{2(1-\theta)}. \tag{6}$$

We stress that h, defined this way, is not a parameter of the model. It merely expresses the conservation of mass of the fluorescent molecules, independently of the model one might choose to describe the diffusion process. We further discuss the choice of a piecewise constant initial datum. We also give a numerical example that supports such a choice in the Appendix.

The solution $u(x, t)$ of the system in Eqs. 2–4 is given in the Appendix. A theoretical recovery function $F(t; D)$, depending on the unknown parameter D, is derived by integrating $u(x, t)$ weighted with the function from Eq. 1. The parameter D is recovered by fitting $F(t;D)$ to the experimental data $F_{\mathrm{data}}(t_i)$, $i = 1,2,\ldots,n$.

Diffusion in the presence of binding and unbinding to an immobile structure

Suppose that fluorescent molecules are divided into two species $u(x, t)$ and $v(x, t)$, called mobile and immobile, respectively. It is assumed that the diffusion region contains an underlying, uniformly distributed immobile structure, consisting of potential binding sites, to which fluorescent molecules can bind with rate k_1 and can be released from with rate k_2. Thus, $v(x, t)$ denotes the bound fraction and $u(x, t)$ is the unbound fraction. The process is renormalized so that the total steady-state concentration $u + v$ before the bleaching process is 1. It is also assumed that the spatially homogeneous immobile structure always contains enough free binding sites so that saturation does not occur (7). The three-parameter model is

$$\frac{\partial}{\partial t}u(x,t) = D\frac{\partial^2}{\partial x^2}u(x,t) - k_1u(x,t) + k_2v(x,t), \tag{7}$$

$$\frac{\partial}{\partial t}v(x,t) = k_1u(x,t) - k_2v(x,t), \tag{8}$$

$$\frac{\partial}{\partial x}u(0,t) = \frac{\partial}{\partial x}u(\ell,t) = \frac{\partial}{\partial x}v(0,t) = \frac{\partial}{\partial x}v(\ell,t) = 0, \tag{9}$$

$$u(x,0) = \frac{k_2}{k_1+k_2}\begin{cases}1 & \text{if } |x-c| > h\\ \theta & \text{if } |x-c| \le h\end{cases}, \tag{10}$$

$$v(x,0) = \frac{k_1}{k_1+k_2}\begin{cases}1 & \text{if } |x-c| > h\\ \theta & \text{if } |x-c| \le h\end{cases}, \tag{11}$$

where c, h, and θ are as in the preceding section. The coefficient D is the diffusion constant and k_1 and k_2 are the reaction rates of the binding and unbinding reactions, respectively. The choice of the initial distributions 10 and 11 is based on the assumption that an equilibrium between bound and unbound molecules has been achieved before the bleaching process, i.e., u and v are in steady state (9). If $k_1 = 0$, the model reduces to the diffusion model (see Eqs. 2–4). In this sense, the one-parameter free-diffusion model (Eqs. 2–4) is nested in the three-parameter reaction-diffusion model (see Eqs. 7–11). This fact will be exploited to discuss the statistical significance of the parameter k_1.

A solution to the model in Eqs. 7–11 is provided in the Appendix. A theoretical recovery function $F(t; D, k_1, k_2)$ is derived in terms of the unknown parameters $\{D, k_1, k_2\}$. These are recovered by fitting $F(t;D, k_1, k_2)$ to the experimental data $F_{\mathrm{data}}(t_i)$, $i = 1,2,\ldots,n$.

Diffusion of particles of different mobilities

Assume that a fraction u of the fluorescent molecules has diffusion constant D_1 and another fraction v has diffusion constant D_2. The model equations are

$$\begin{aligned}
\frac{\partial}{\partial t}u(x,t) &= D_1\frac{\partial^2}{\partial x^2}u(x,t) \quad x \in (0,\ell), t \ge 0,\\
\frac{\partial}{\partial t}v(x,t) &= D_2\frac{\partial^2}{\partial x^2}v(x,t) \quad x \in (0,\ell), t \ge 0,\\
\frac{\partial}{\partial x}u(0,t) = \frac{\partial}{\partial x}u(\ell,t) &= \frac{\partial}{\partial x}v(0,t) = \frac{\partial}{\partial x}v(\ell,t) = 0, t \ge 0,\\
\alpha u(x,0) + (1-\alpha)v(x,0) &= \begin{cases}1 & \text{if } |x-c| > h\\ \theta & \text{if } |x-c| \le h.\end{cases}
\end{aligned} \tag{12}$$

Here, $\alpha \in [0, 1]$ denotes the fraction that has diffusion constant D_1. The total fluorescence is then a convex combination

$$F_3(t; D_1, D_2, \alpha) = \alpha F_1(t; D_1) + (1-\alpha)F_1(t; D_2), \tag{13}$$

where F_1 denotes the recovery function of simple diffusion given in Eq. 17.

RESULTS

Validation of the p53-GFP fusion protein

To ensure that the p53-GFP fusion protein was able to bind DNA and activate transcription similar to unmodified p53, we examined the ability of the p53-GFP fusion protein to

upregulate p53 target genes. Ectopic expression of the p53-GFP fusion protein resulted in elevated levels of the p53 target gene products, p21 and mdm2, in a manner comparable to unmodified p53 protein (Fig. 2). These data demonstrate that the p53-GFP fusion protein retains proper DNA binding and transcriptional activation capabilities. Furthermore, p53-GFP is correctly targeted to the nucleus of H1299 cells (Fig. 3). Since the subcellular distribution and biochemical activities of the p53 fusion protein are intact, this protein is a valid probe for imaging of p53 nuclear dynamics. Note, the H1299 cells are null for p53, thus the only p53 protein expressed in the cells is that which is ectopically expressed after transfection of the p53-GFP expression vector.

Checking for immobile fractions

We next determined if p53-GFP behaves as a mobile or immobile protein. To test for the presence of an immobile fraction, we performed confocal FRAP experiments on H1299 cells expressing p53-GFP (see Appendix for details). In the first series of experiments, we bleached a strip across the nucleus twice in succession (23). If an immobile fraction is present it should be bleached completely the first time within the bleach strip but remain unaffected elsewhere. During the second bleach of the same strip, only mobile molecules will be bleached.

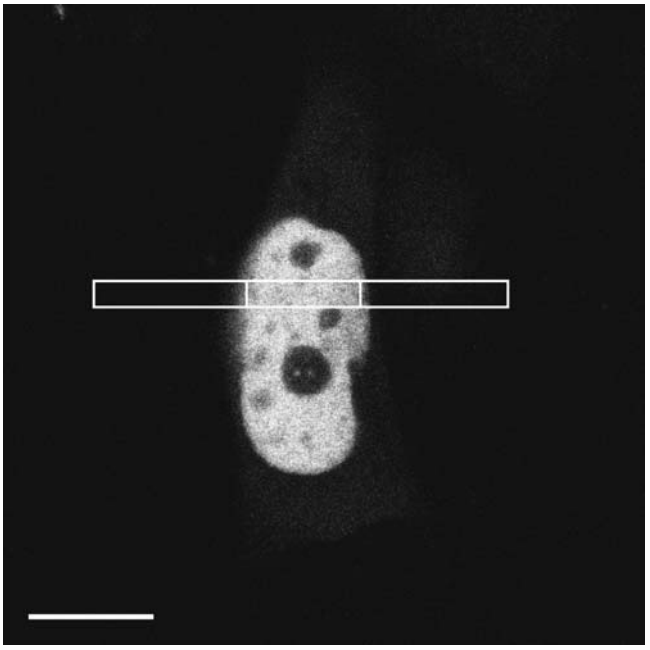

FIGURE 3 A nucleus of a H1299 lung cancer cell expressing with p53-GFP. The bleach strip is shown in white.

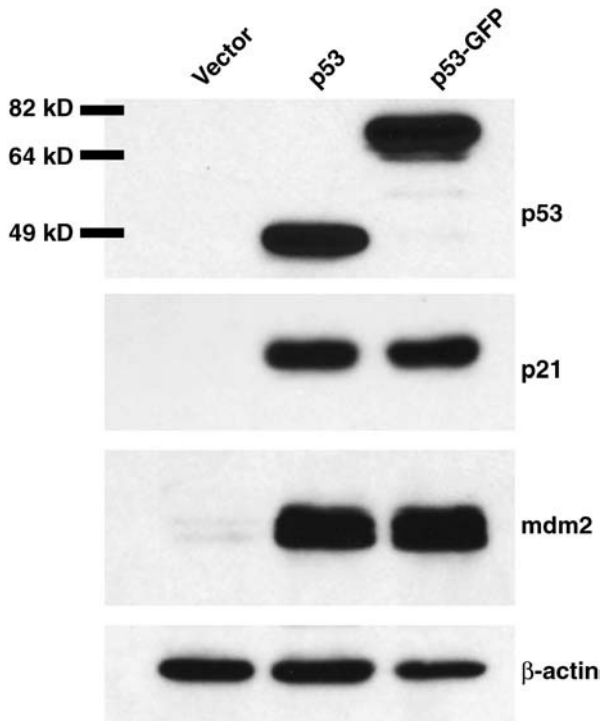

FIGURE 2 Expression of the p53-GFP fusion protein results in elevation of p53 target genes products similar to unmodified p53. H1299 cells were transfected with an empty vector, or an expression vector encoding p53 or p53-GFP fusion proteins. Twenty-four hours after transfection, cells were harvested, and protein levels of p53, p21, and mdm2 were determined by Western analysis. The β-actin protein levels are shown as a loading control. Results are representative of at least three independent experiments.

We designate the ultimate (asymptotic) level of recovery measured after the first and the second bleaching procedure as F_1 and F_2, respectively. Let β be the normalized volume of a possible immobile fraction. By the theoretical arguments (see Appendix), based on conservation of mass, one has $F_2^2/F_1 = (1-\beta)$. The experimental data, however, give $F_2^2/F_1 \approx 1$, which yields $\beta \approx 0$ and provides evidence against the presence of an immobile fraction (Fig. 4). Thus, we attribute the loss of fluorescence solely to the bleaching and do not assume the existence of an immobile p53-GFP fraction on the timescale of the experiment ($\approx$1 min).

A second test for immobile fractions was conducted by bleaching a circular spot and measuring the asymptotic, normalized fluorescence at the bleach spot, and at another, unbleached circular region of equal radius, disjoint from the bleach spot, but within the same domain of diffusion (19). Let F_1 and F'_1 be their ultimate recovery levels. Conservation of mass implies (see Appendix) $\beta = F'_1 - F_1$, whereas the data give $F'_1 \approx F_1$ (Fig. 5). Thus $\beta \approx 0$.

The diffusional mobility of GFP versus p53-GFP

Having determined that p53-GFP is fully mobile, we next assessed its diffusional mobility compared to that of GFP alone. Representative recovery curves obtained for p53-GFP

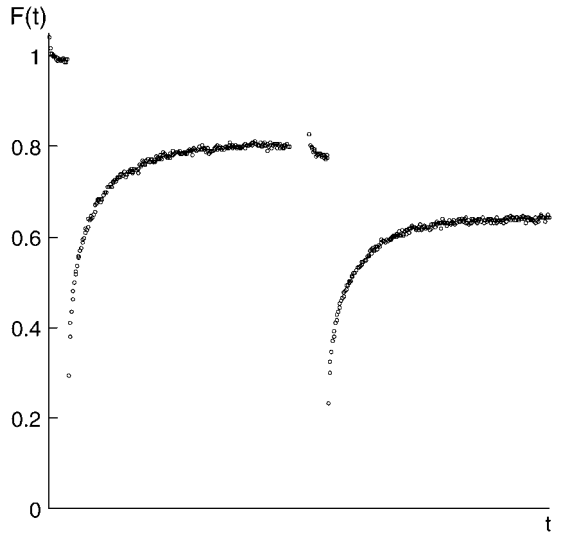

FIGURE 4 Repeated bleaches of p53-GFP in the same region, ~1-min apart. The recovery took ~20 s each time. The observed levels of recovery are $F_1 = 0.8033$ after the first bleach and $F_2 = 0.6434$ after the second bleach. It follows from Eq. 24 that $\beta = 0$, i.e., the data do not suggest the existence of an immobile fraction on the timescale of 1 min. This experiment was performed three times with similar results.

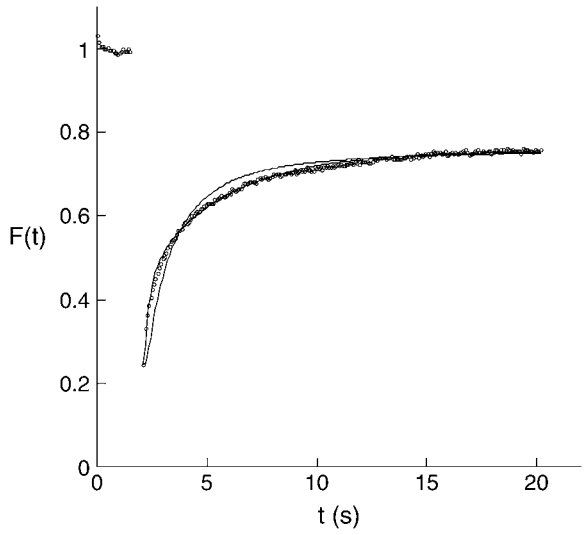

FIGURE 6 A representative fluorescence recovery curve for p53-GFP. Shown are the optimal fits with the one-parameter model (Eqs. 2–4, and 17, poor fit) and with the three-parameter model (Eqs. 7–11, and 22, close fit). The values of the optimal parameters are $D = 20.5\ \mu m^2\ s^{-1}$, $k_1 = 0.257\ s^{-1}$, and $k_2 = 0.318\ s^{-1}$. Notice that the residuals of the optimal fit with the one-parameter model are bimodal.

and GFP in the nucleus are shown in Figs. 6 and 7, respectively. The standard deviation of the measurement noise was determined to be $\sigma = 0.01161$ (see Appendix). We first tried to fit all curves with the theoretical recovery function $F_1(\cdot;D)$ from the one-parameter model (Eq. 17). The average effective diffusion constant obtained from the one-parameter model was $D_{\text{eff, p53–GFP}} = 6.2\ \mu m^2\ s^{-1}$. However, apart from a few exceptional cases, the one-parameter diffusion model was not able to explain the experimental data satisfactorily (Fig. 6). We took this as reason to reject the one-parameter diffusion model for p53-GFP.

We then proceeded to fit the theoretical recovery function $F_2(\cdot;D, k_1, k_2)$, obtained from the three-parameter model (Eq. 22) to the p53-GFP recovery curves (Table 1). For GFP, on the other hand, in 7 out of 10 cases the one-parameter model provided an acceptable fit of the experimental data (Fig. 7).

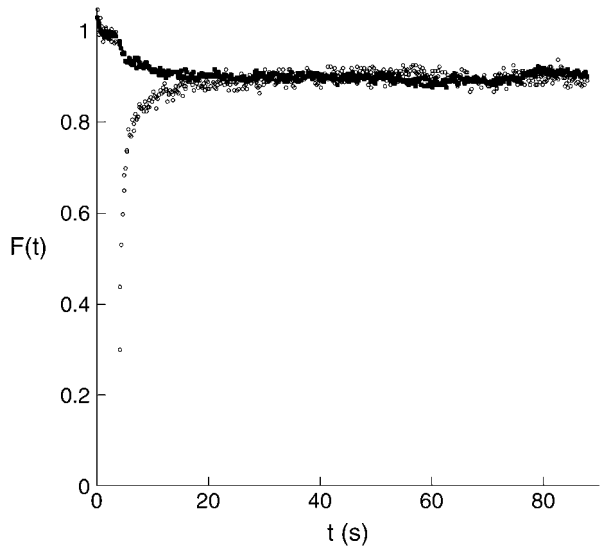

FIGURE 5 Observation of fluorescence of p53-GFP at a circular bleach spot and a disjoint circular spot in the same nucleus (*lower* and *upper curves*, respectively). The ultimate levels of the normalized fluorescence match, i.e., $\beta = 0$ from Eq. 25. These data are representative of four independent experiments.

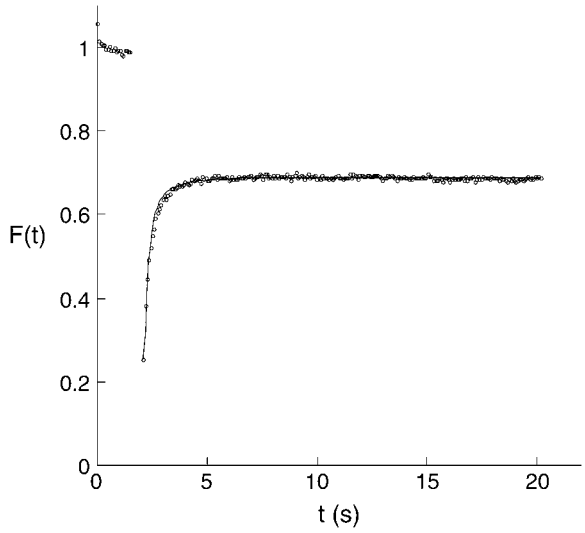

FIGURE 7 A representative fluorescence recovery curve for GFP. Shown is the optimal fit with the one-parameter model (Eqs. 2–4, and 17). The optimal parameter value is $D = 66.3\ \mu m^2\ s^{-1}$.

Therefore, we accept the hypothesis that GFP is freely diffusing inside the cells.

The diffusion constant obtained for GFP in the nucleus (Table 1) is in close agreement with in vivo values published in the literature, e.g., $D = 43 \pm 11\ \mu m^2\ s^{-1}$ (24) and $D = 58 \pm 9\ \mu m^2\ s^{-1}$ (25) (although smaller values at $\sim 15\ \mu m^2\ s^{-1}$ have also been reported; (7) and references therein).

The analysis of our recovery data for p53-GFP with the two-component model from Eqs. 12 and 13 yields a slow fraction with $\alpha = 0.66$ and $D_1 = 3.78\ \mu m^2\ s^{-1}$ and a fast fraction with $D_2 = 84.6\ \mu m^2\ s^{-1}$. These values are averages of 11 out of 12 runs performed on Day 2. Of course, the two-component model too yields a much better fit than the simple diffusion model and would have to be accepted on purely statistical grounds. However, it would imply that the fast fraction diffuses twice as fast as GFP alone, and further, that the ratio of the masses of the heavy and the light particles would be of the order of 10^4, according to Eq. 14 below. Based on these physical considerations, we reject the two-component model as a possible explanation of the fluorescence recovery data for p53-GFP.

We tested whether the introduction of the extended model (Eqs. 7–11) improves the fit of the recovery data for p53-GFP in a statistically significant way. The procedure is described in the Appendix, where a concrete numerical example is also given. Overall, at a confidence level $\alpha = 0.1$, the null-hypothesis $k_1 = 0$ can be rejected in 35 out of 58 cases and at a confidence level $\alpha = 0.06$, in 31 out of 58 cases. This indicates the significance of the binding rate constant k_1.

The diffusional mobility of p53-GFP DNA binding mutants

The values of k_1 and k_2 obtained for p53-GFP using the reaction-diffusion model are suggestive of weak, nonspecific binding (7). To further test the contribution of specific DNA binding events to the apparent diffusion of p53-GFP, we performed FRAP experiments using tumor-derived p53 mutants that are deficient in sequence-specific DNA binding activity, R175H and R273H (arginine → histidine). The central domain of p53 (amino acids 100–292) is required for the protein to interact with DNA in a sequence-specific manner (26). Solution of the crystal structure of p53 demonstrated that the central domain of p53 consists of a β-sandwich that serves as a scaffold for two large loops and a loop-sheet-helix motif. The two loops are held together by a coordinated zinc atom, and the loop-sheet-helix motif forms the DNA binding surface of p53 (27). The two tumor-derived mutants analyzed in this study represent two different classes of mutant proteins containing point mutations in their DNA binding domain. The R175H mutation results in major disruption of the domain's structure and loss of coordination of the zinc atom, whereas the R273H mutation only disrupts the DNA binding surface of the molecule without affecting overall structure of the central domain.

Like p53-GFP, both p53 R175H-GFP and p53 R273H-GFP were targeted to the nucleus (data not shown). Approximately 40 FRAP experiments were carried out on each mutant protein, using the same experimental setup as for the wild-type p53-GFP. For both mutants, the one-parameter model was insufficient to fit the recovery curves, whereas the three-parameter model provided an excellent fit. Significantly, the parameters of the three-parameter fit were identical within error for those obtained for the sequence-specific DNA-binding mutants and the wild-type p53 fusion protein (Table 1). This further substantiates the notion that specific DNA binding does not contribute significantly to the slowed diffusion of p53-GFP compared to GFP.

DISCUSSION

In this work, we have examined the nuclear diffusional mobility of p53-GFP using confocal FRAP. We show that p53-GFP is fully mobile, but exhibits slowed diffusion compared to GFP alone. We find that a free diffusion model is sufficient to explain the diffusional mobility of free GFP in the nucleus. In contrast, p53-GFP exhibited more complex behavior consistent with a reaction-diffusion model, in which free diffusion is coupled with binding and release from an immobile structure.

The lack of a difference between the diffusion properties of wild-type and the tumor-derived mutant p53 proteins from these two classes suggests that, under steady-state conditions, the protein binds DNA in a sequence-independent manner and regions of the protein besides the central domain are required for this interaction. Consistent with our findings are previous fluorescence correlation spectroscopy studies showing that p53 is a latent DNA binding protein that must become activated for sequence-specific DNA binding (15). In fact, Wölcke et al. (15) show that the nonspecific binding of p53 to DNA requires the C-terminus of the protein, thus perhaps explaining the similarity of wild-type and mutant p53 proteins, since they both have intact C-termini.

The physiological significance of nonspecific DNA includes the following possibilities:

1. For initiation of transcriptional activation of p53 regulated genes, the nonspecific interaction may keep p53 tightly associated with DNA and minimize time of binding or stabilize p53 binding to sequence-specific sites (8).
2. It may serve to maintain a given threshold level of p53 in the genome for rapid activation.
3. It may assist in functions of p53 in chromatin remodeling that are separate from the protein's role in sequence-specific transactivation (28–30).

Evidence that p53-GFP is fully mobile

Our data provide evidence against the existence an immobile fraction for p53-GFP. (This is not to be confused with

immobile structure, whose presence here we reassert on statistical grounds.) Immobile fractions have been suggested as a way of explaining the discrepancy between the observed, experimental partial recovery, versus the corresponding theoretical full recovery of fluorescent molecules. These theoretical recovery functions (31) are based on assuming that the diffusion domain is the entire, either two- or three-dimensional space. However, for small compartments like the nucleus, a significant fraction of material may be lost due to the bleach. In this case, the physically more realistic notion of a bounded, insulated, diffusion region (for example, a rectangle), coupled with the flexibility in the choice of the initial density profiles, permits us to match theoretical and experimental recovery profiles. These arguments are based on considerations of conservation of mass in bounded insulated regions (see Appendix). In unbounded diffusion regions, by renormalizing the initial density profile of fluorescent particles to 1, the mass is theoretically infinite at all times, and thus insensitive to losses due to the beaching process. Thus, theoretically, the time-asymptotic density distribution will be 1, whereas the asymptotic experimental total mass will consist of the actual initial mass minus that portion lost to the bleaching process.

It is important to make this correction for small compartments like the nucleus where a significant fraction of material may be lost due to the bleach. Otherwise, one may erroneously conclude that an immobile fraction is present.

Biological significance of the observed free diffusion coefficient and binding rate constants for p53-GFP

A hallmark of a protein undergoing constrained diffusion is an unexpectedly small diffusion coefficient. For example, Phair and Misteli (6) have reported effective diffusion constants of the order $D \approx 0.5\ \mu m^2\ s^{-1}$ for a GFP-tagged nucleosomal binding protein, a splicing factor, and an rRNA processing protein. These values are two orders-of-magnitude smaller than the diffusion constant of GFP alone, a clear indication of a mechanism different from free Brownian motion. The value $D = 0.073\ \mu m^2\ s^{-1}$ reported by Carrero et al. (9,11) for the nuclear histone H1 indicates a strong binding to an immobile structure as well, as would be expected of a building block of chromatin. Similarly, when we fit the FRAP data for p53-GFP with a free diffusion model, we obtained a slow effective diffusion coefficient, $6.2\ \mu m^2\ s^{-1}$. Moreover, we found that the single-parameter/free diffusion model yielded poor fits to the experimental recovery curves (Fig. 6). Taken together, these two observations strongly suggest that p53-GFP does not undergo free diffusion in the nucleus. Even when we assumed the presence of two freely diffusing species, we could not account for the observed diffusion unless we assumed a difference in 10^4 in molecular weight between the two species, a highly implausible scenario. In contrast, our analysis indicates that the diffusional mobility of p53-GFP in the nucleus is well described by a reaction-diffusion model in which the protein binds and releases from an immobile structure. This model contains several parameters: a free diffusion coefficient of the unbound species, and binding and unbinding rates k_1 and k_2, respectively.

The free diffusion coefficient for p53-GFP obtained from the reaction-diffusion model suggests that p53-GFP diffuses as an oligomer rather than a monomer. The free diffusion coefficients D_1 and D_2 of two spherical proteins of molecular weights m_1 and m_2 are linked by the formula below (7):

$$\frac{D_1}{D_2} = \left(\frac{m_2}{m_1}\right)^{\frac{1}{3}}. \tag{14}$$

The mass of GFP has been reported to be $m_{GFP} = 27$ kg/mole (32). We estimate the mass of a single p53-GFP molecule to be $53 + 27 = 80$ kg/mole (see also Fig. 2). Using the averages $D_{p53\text{-}GFP} = 15\ \mu m^2\ s^{-1}$ and $D_{GFP} = 40\ \mu m^2\ s^{-1}$ in Eq. 14 one can calculate the mass of the diffusing p53-GFP particles to be

$$m_{p53-GFP} = m_{GFP}\left(\frac{D_{GFP}}{D_{p53-GFP}}\right)^3 > 500\text{kg/mole}.$$

This mass suggests that p53-GFP is present in an oligomerized form in the cell nucleus. This estimate is robust qualitatively, in the sense that even assuming a smaller diffusion constant for GFP, say $D_{GFP} = 30\ \mu m^2\ s^{-1}$ would still give a mass $m_{p53\text{-}GFP} > 200$ kg/mole, again indicating the presence of an oligomerized form. We want to stress, however, that this can serve only as a plausibility argument, since no information is presently available about the shape of the p53-GFP construct. Nonetheless, our data are consistent with early studies showing the predominant form of native, immunopurified p53 is a tetramer and that these tetramers can bind directly to DNA (33). Further, the oligomerization domain resides in the carboxy-terminal domain of the protein and thus would be intact in both the wild-type p53-GFP and tumor-derived p53-GFP proteins analyzed in this study. Several studies have convincingly shown that oligomerization is important for regulation of p53 transcriptional and tumor-suppressive activities (34,35).

It is well known that transcription factors bind nonspecifically to DNA, in addition to tight binding to their promoter sites. Sprague et al. (7) have termed release rate constants k_2 at $\sim 10\ s^{-1}$ as typical for nonspecific DNA binding whereas values near $10^{-6}\ s^{-1}$ indicate specific binding. We are aware that our system overexpresses p53-GFP to some degree. Nevertheless, we take our value $k_2 = 0.4\ s^{-1}$ as a sign of nonspecific DNA binding of unmodified p53. This conclusion is supported by our observation that the diffusional mobility of DNA binding mutants and wild-type p53-GFP are identical within error (Table 1). For comparison, Sprague et al. (7) estimate a binding rate $k_1 = 500\ s^{-1}$ and a release rate $k_2 = 86.4\ s^{-1}$ for GFP-tagged glucocorticoid receptor (GFP-GR). Finally, we note that while the reaction-diffusion

TABLE 1 The mean parameter values together with their standard deviations are shown; notice that the diffusion constant reported for GFP is that of the one-parameter model

Protein	D ($\mu m^2\ s^{-1}$)	k_1 (s^{-1})	k_2 (s^{-1})
GFP	41.6 ± 13.6	—	—
p53-GFP	15.4 ± 5.6	0.31 ± 0.22	0.40 ± 0.13
R175H-GFP	17.9 ± 8.6	0.41 ± 0.30	0.41 ± 0.13
R273H-GFP	17.6 ± 8.2	0.39 ± 0.22	0.34 ± 0.12

model is a natural choice for describing such behavior in terms of binding and unbinding events, a variety of other mechanisms can also impede free diffusion of proteins in living cells (36).

The geometrical setup and the choice of the initial datum to the recovery process

It is a general difficulty of FRAP experiments to find a suitable geometric approximation to the domain in which the diffusion takes place. Not only are nuclei not rectangles, they also contain macroscopic bodies such as, for example, nucleoli, Cajal bodies, and others that complicate the assumption of a spatially homogeneous nucleus. We think, however, that the one-dimensionalized model is acceptable, since the estimated diffusion and reaction rate constants are consistent across different cells and reproducible.

The initial datum is the resulting density profile of the p53-GFP fusion at completion of the photobleaching process. Here it is taken to be piecewise constant. The problem of finding the right initial datum for the recovery process is still a point of investigation. Assume, as proposed previously by Axelrod et al. (31), that photobleaching is a first-order chemical reaction with reaction constant $\kappa I(x)$, where I denotes the intensity profile of the laser beam. The constant $\kappa > 0$ is the photobleach constant of the fluorescent substance. The bleaching laser beam is turned on at time $-T_{\mathrm{bl}}$, it is turned off at time 0, and the fluorescence is subsequently observed until time T_{end}. Denote by $\tilde{u}(x,t)$ the concentration of fluorescent molecules at $x \in (0, \ell)$ and time $t \in (-T_{\mathrm{bl}}, T_{\mathrm{end}})$. The combined process of bleaching and diffusion in the domain $(0, \ell)$ for the whole time lapse $(-T_{\mathrm{bl}}, T_{\mathrm{end}})$, assuming free diffusion (i.e., no binding-unbinding effects to possible immobile structures), can be described by

$$\begin{aligned}
\frac{\partial}{\partial t}\tilde{u}(x,t) &= D\frac{\partial^2}{\partial x^2}\tilde{u}(x,t) - \chi_{[-T_{\mathrm{bl}},0]}(t)\kappa I(x)\tilde{u}(x,t)\\
\frac{\partial}{\partial x}\tilde{u}(0,t) &= \frac{\partial}{\partial x}\tilde{u}(\ell,t) = 0\\
\tilde{u}(x,-T_{\mathrm{bl}}) &= 1,
\end{aligned} \tag{15}$$

where the uniform initial concentration is set to unity. The boundary conditions on $x = 0$ and $x = \ell$ are of zero flux, as in Eq. 3. The indicator function

$$\chi_{[-T_{\mathrm{bl}},0]}(t) = \begin{cases} 1 & \text{if } -T_{\mathrm{bl}} \le t \le 0 \\ 0 & \text{otherwise} \end{cases}$$

represents the switching of the bleaching laser beam. The profile of $\tilde{u}(\cdot,0)$ at $t = 0$ is, at least theoretically, the physical initial datum to be associated to Eqs. 2 and 3 instead of Eq. 4, i.e.,

$$\tilde{u}(\cdot,0) = u(\cdot,0).$$

For such a choice, Eqs. 2 and 3 produce a solution $u(x, t)$ that for all $t \ge 0$, coincides with the solution $\tilde{u}(x,t)$ of the system in Eq. 15. Solving the system in Eq. 15 does not require the knowledge of $\tilde{u}(\cdot,0)$. This suggests we should dispense with the issue of the initial datum altogether, as follows. First, one would solve system Eq. 15 and construct the theoretical recovery function $\tilde{F}(t;D)$ by integrating $\tilde{u}(\cdot,t)$ against the intensity profile. Then one would fit the experimental recovery curves against this theoretical recovery function. Although the procedure is theoretically correct, it hinges upon the knowledge of the parameter κ and the intensity profile $I(\cdot)$ of the laser beam.

Thus avoiding the knowledge of $u(\cdot, 0)$ is traded with the a priori knowledge of other parameters, such as κ, which might be harder to estimate.

Our choice of a piecewise constant initial datum, as in Eq. 4, introduces two parameters h and θ. However, they are determined by the very same experiment whose recovery curve we seek to fit. In addition, the determination of h in Eqs. 5 and 6, is based on first principles only and it is independent of the diffusion model.

It remains to discuss whether a piecewise constant profile suitably approximates the true physical initial profile. We have addressed this point by providing numerical evidence that equal mass solutions of system Eqs. 2–4 and 15 are close (see Appendix, and Figs. 8 and 9).

Statistical analysis of model acceptance

A novel contribution of our analysis is the statistical analysis of acceptance or rejection of a model, as opposed to a statistical test of accepting or rejecting a specific value of a parameter. It has already been observed that the free diffusion model can be obtained from the reaction-diffusion model for the choice of the parameter $k_1 = 0$. This is a particular case of a family of nested models, i.e., an ordered, finite collection of models. Roughly speaking, models of this family are generated by a preceding model by the inclusion of further hypotheses and parameters, in such a way that the preceding model is a particular case of the subsequent model, for special choices of the parameters. For such families, Banks and Fitzpatrick (20) have introduced a statistical method to test the significance of the subsequent model with respect to the preceding one. Given a model, how statistically significant is it to expand the model by introducing new mechanisms and parameters? The statistical method of Banks and Fitzpatrick (20) was applied to test the significance of the binding rate constants k_1. It was found that the diffusion of p53-GFP

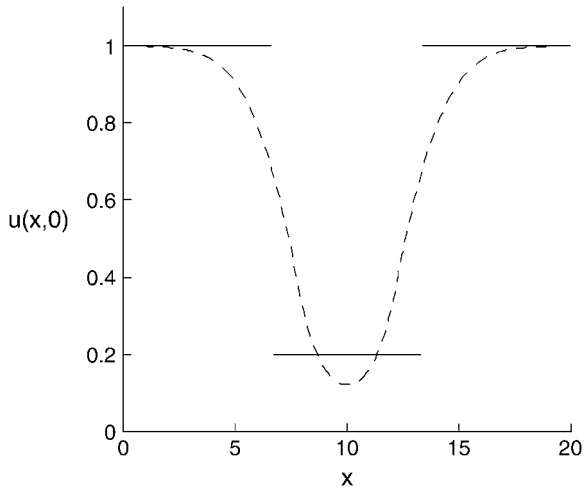

FIGURE 8 Initial data at the end of the bleach time in presence of diffusion into the bleach spot. The reaction-diffusion system Eq. 15 is solved numerically on the domain $(x, t) \in [0, 20] \times [-0.5, 20]$ with chosen parameters $D = 6.0$ and $\kappa = 6.0$. Homogeneous Neumann boundary conditions $\tilde{\boldsymbol{u}}_x(0,t) = \tilde{\boldsymbol{u}}_x(\ell,t) = 0$ are imposed. The normalized uniform fluorescence intensity profile I is from Eq. 1 with $r = 2.2$ and $c = 10$. Shown are the true initial datum for the recovery $\tilde{u}(x,0)$ (*dashed line*) and the estimated initial datum (*solid line*). The bleach depth was determined to be $\theta = \int_0^\ell \tilde{u}(x,0)I(x)\mathrm{d}x = 0.1984$ by numerical integration. The ultimate level of recovery was found to be $\tilde{F}_\infty = \tilde{F}(T_{\text{end}}) = 0.7301$ (Fig. 9). With these values, it follows from Eq. 6 that $h = 3.37$. (This is called the ''corona effect'' in (13)).

cannot be explained by the free diffusion alone ($k_1 = 0$). Indeed, such an hypothesis cannot be reconciled with the experimental data, by statistical test (20). This suggests that k_1 must be nonzero and provides quantitative evidence to the notion of binding to immobile structures (see Appendix). This method of model discrimination can be applied to any protein, nuclear or otherwise, that is suspected to undergo binding events, provided that the mathematical models in use are nested.

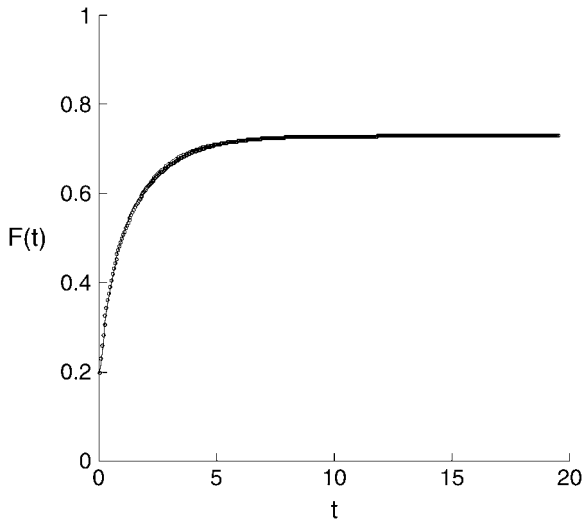

FIGURE 9 The fluorescence recovery is fitted with Eq. 17. The initial datum estimated according to Eq. 6 ($h = 3.37, \theta = 0.1984$) gives $D = 6.5375$ (*dotted line*). The actual recovery $\tilde{F}(t)$ with the true diffusion constant $D = 6.0$ is shown (*thin solid line*). Notice that the time is measured in arbitrary units.

APPENDIX

The model for free diffusion

The unique solution to Eqs. 2–4 is found by separation of variables (37). Let

$$\lambda_0 = 0, \quad \varphi_0(x) = \left(\frac{1}{\ell}\right)^{\frac{1}{2}},$$

$$\lambda_j = \left(\frac{\pi j}{\ell}\right)^2, \quad \varphi_j(x) = \left(\frac{2}{\ell}\right)^{\frac{1}{2}} \cos\frac{\pi j x}{\ell}, \quad j = 1, 2.$$

Denote the eigenvalues and normalized eigenfunctions of the Laplace operator on $(0, \ell)$, with homogeneous Neumann boundary conditions. Then the solution to Eqs. 2–4 is given by the series

$$\begin{aligned} u(x,t) &= \sum_{j=0}^{\infty} \exp(-\lambda_j D t)\left(\int_0^\ell u(\xi,0)\varphi_j(\xi)\mathrm{d}\xi\right)\varphi_j(x) \\ &= \frac{\ell - 2h(1-\theta)}{\ell} + \frac{2(1-\theta)}{\pi}\sum_{j=1}^{\infty}\exp\left(-\frac{\pi^2 j^2 D t}{\ell^2}\right)\frac{1}{j} \\ &\quad \times \left[\sin\frac{j\pi(c-h)}{\ell} - \sin\frac{j\pi(c+h)}{\ell}\right]\cos\frac{\pi j x}{\ell}. \end{aligned} \tag{16}$$

Multiplying the series in Eq. 16 by the intensity profile 1, integrating over $[0, \ell]$, and dividing by $2r$, gives the theoretical recovery function

$$\begin{aligned} F_1(t;D) &= \frac{1}{2r}\int_{c-r}^{c+r} u(x,t)\mathrm{d}x \\ &= \frac{\ell - 2h(1-\theta)}{\ell} + \frac{\ell(1-\theta)}{r\pi^2} \times \sum_{j=1}^{\infty}\exp\left(-\frac{\pi^2 j^2 D t}{\ell^2}\right) \\ &\quad \times \frac{1}{j^2}\left[\sin\frac{j\pi(c-h)}{\ell} - \sin\frac{j\pi(c+h)}{\ell}\right] \\ &\quad \times \left[\sin\frac{j\pi(c+r)}{\ell} - \sin\frac{j\pi(c-r)}{\ell}\right]. \end{aligned} \tag{17}$$

From this, one computes the ultimate (asymptotic) level of recovery as

$$F_{1,\infty} \overset{\text{def}}{=} \lim_{t\to\infty} F(t;D) = 1 - \frac{2h(1-\theta)}{\ell} < 1. \tag{18}$$

The reaction-diffusion model

The system in Eqs. 7–11 is solved by separation of variables by seeking its unique solution in the form

$$u(x,t) = \sum_{j=0}^{\infty} u_j(t)\varphi_j(x), \quad v(x,t) = \sum_{j=0}^{\infty} v_j(t)\varphi_j(x), \tag{19}$$

where $t \to u_j(t)$, $v_j(t)$ are to be determined from Eqs. 7 and 8, with initial conditions

$$u_j(0) = \int_0^\ell u(x,0)\varphi_j(x)\mathrm{d}x, \quad v_j(0) = \int_0^\ell v(x,0)\varphi_j(x)\mathrm{d}x.$$

The Laplace transform of $u_j(\cdot)$ and $v_j(\cdot)$ is

$$\bar{u}_j(s) = \int_0^\infty e^{-st}u_j(t)\mathrm{d}t, \quad \bar{v}_j(s) = \int_0^\infty e^{-st}v_j(t)\mathrm{d}t.$$

Put Eq. 19 into Eqs. 7 and 8, multiply by $\varphi_i(x)$ for a fixed index i, integrate in dx over $(0, \ell)$, and take the Laplace transform of the resulting term. This gives

$$s\bar{u}_j(s) - u_j(0) = -\left(\frac{j\pi}{\ell}\right)^2 D\bar{u}_j(s) - k_1\bar{u}_j(s) + k_2\bar{v}_j(s),$$
$$s\bar{v}_j(s) - v_j(0) = k_1\bar{u}_j(s) - k_2\bar{v}_j(s).$$

Solving for $u_j(s)$ and $v_j(s)$ yields

$$\bar{u}_j(s) = \frac{(s+k_2)u_j(0) + k_2v_j(0)}{(s+(j\pi/\ell)^2D+k_1)(s+k_2) - k_1k_2},$$
$$\bar{v}_j(s) = \frac{(s+(j\pi/\ell)^2D+k_1)v_j(0) + k_1u_j(0)}{(s+(j\pi/\ell)^2D+k_1)(s+k_2) - k_1k_2}, \qquad (20)$$

provided the denominator of these fractions is nonzero. The solutions of the equation

$$(s+(j\pi/\ell)^2D+k_1)(s+k_2) - k_1k_2 = 0$$

are

$$s_{1,2;j} = -\frac{(j\pi/\ell)^2D+k_1+k_2}{2} \pm \frac{\sqrt{((j\pi/\ell)^2D+k_1+k_2)^2 - 4k_2(j\pi/\ell)^2D}}{2}.$$

After a partial fraction decomposition of Eq. 20, the Laplace transform can be inverted to give

$$\begin{aligned} u_j(t) &= (s_{1;j} - s_{2;j})^{-1} \\ &\quad \times([u_j(0)s_{1;j} + k_2(u_j(0)+v_j(0))]e^{s_{1;j}t} \\ &\quad -[u_j(0)s_{2;j} + k_2(u_j(0)+v_j(0))]e^{s_{2;j}t}), \\ v_j(t) &= (s_{1;j} - s_{2;j})^{-1} \\ &\quad \times([v_j(0)(s_{1;j} + (j\pi/\ell)^2D+k_1) + k_1u_j(0)]e^{s_{1;j}t} \\ &\quad -[v_j(0)(s_{2;j} + (j\pi/\ell)^2D+k_1) + k_1u_j(0)]e^{s_{2;j}t}). \end{aligned} \qquad (21)$$

Both species are fluorescent and contribute to the normalized signal

$$\begin{aligned} F_2(t;D,k_1,k_2) &= \frac{1}{2r}\int_0^\ell [u(x,t)+v(x,t)]I(x)\mathrm{d}x \\ &= \frac{1}{2r}\int_{c-r}^{c+r}[u(x,t)+v(x,t)]\mathrm{d}x. \end{aligned} \qquad (22)$$

To summarize, the theoretical recovery function is computed by first inserting the $u_j(\cdot)$ and $v_j(\cdot)$ computed in Eq. 21, into the expressions in Eq. 19, and then by inserting the resulting $u(x,t)$ and $v(x,t)$ into Eq. 22. Since $s_{1;0} = 0$ and all other $s_{1,\,2;k}$ values are negative, we compute the ultimate (asymptotic) level of recovery as

$$F_{2,\infty} \overset{\text{def}}{=} \lim_{t\to\infty} F_2(t;D,k_1,k_2) = 1 - \frac{2h(1-\theta)}{\ell},$$

which is the same as that in Eq. 18 for the free diffusion model. Observe further that in case $k_1 = 0$ we have for all k_2, $\tilde{k}_2$:

$$F_2(t;D,0,k_2) = F_2(t;D,0,\tilde{k}_2) = F_1(t;D). \qquad (23)$$

This implies that the level sets of the cost-functional J from Eq. 26 in the plane $\{k_1 = 0\}$ are the lines $\{D = const\}$.

Testing for the presence of an immobile fraction

Before any bleaching the normalized fluorescence intensity is $F_0 = 1$. Assume that the compartment $[0, \ell]$ contains immobile and mobile fluorescent particles, their fractions being β and $1 - \beta$, respectively. Suppose now that an interval of length $2h$ is completely depleted of fluorescent molecules. The recovery is due solely to the mobile fraction, therefore the level of recovery after a sufficiently long time will be (assuming conservation of mass)

$$F_1 = (1-\beta)\frac{\ell-2h}{\ell}.$$

If the same region is now bleached again, only mobile particles will be destroyed. The second recovery will reach a level of

$$F_2 = (1-\beta)\left(\frac{\ell-2h}{\ell}\right)^2.$$

Hence, we have

$$1-\beta = \frac{F_1^2}{F_2} = F_1\left(\frac{\ell}{\ell-2h}\right). \qquad (24)$$

Also, the fluorescence recovery level after the first bleach in a region disjoint to the bleach region will be

$$F_1' = \beta + (1-\beta)\frac{\ell-2h}{\ell},$$

since the immobile molecules were not affected. It follows that

$$\beta = F_1' - F_1. \qquad (25)$$

Notice that the actual size $2h$ of the bleached region in these experiments does not matter.

Statistical issues

For both models, we derive a theoretical recovery function $F(t;q)$ by integrating the solution of the initial value problem weighted with the intensity profile. It depends on the parameter $q = (q_1,\ldots,q_p)$ (where $p = 1$ or $p = 3$). Given are the data points $(t_i, F_{data}(t_i))$, $i = 1,\ldots,n$. We assume the existence of a true parameter which, by definition, is a q^* such that

$$F_{data}(t_i) = F(t_i;q^*) + \varepsilon_i,$$

where the ε_i are independent, identically distributed random variables with mean $E(\varepsilon_i) = 0$ and variance $Var(\varepsilon_i) = \sigma^2 < \infty$. An estimate for q^* is obtained by a least–square fit of $F(t;q)$ to the experimental data. That is, we minimize the cost-functional

$$J(q) = \sum_{i=1}^n (F(t_i;q) - F_{data}(t_i))^2 \to \min_{q\in\mathcal{Q}_{ad}}!, \qquad (26)$$

where n is the number of data points making up the recovery part of the experiment and $\mathcal{Q}_{ad}$ denotes the set of admissible parameters. The set $\mathcal{Q}_{ad}$ can be chosen to be compact. Since the functional J is continuous in q, the existence of a minimizer is guaranteed, denote any such minimizer by $\hat{q}$. An optimal residual $J(\hat{q}) = 0$ is not to be expected since the measurements are afflicted with errors and the model itself is only an approximation.

We now discuss the statistical test for the significance of the parameter k_1. Choose the admissible parameter set $\mathcal{Q}_{ad}$ such that it is compact and that the true parameter lies in its interior (20). Let

$$\mathcal{Q}_0 = \{(D, k_1, k_2) \in \mathcal{Q}_{ad} : k_1 = 0\}$$

be the restricted parameter set. We want to test the null-hypothesis $H_0 : q^* \in \mathcal{Q}_0$. Indeed, as we have seen, fixing the binding rate constant $k_1 = 0$ in Eqs. 7–11 reduces the model to the simple diffusion model Eqs. 2–4. We calculate the statistic

$$U = \frac{J(\tilde{D}, 0, \cdot) - J(\hat{D}, \hat{k}_1, \hat{k}_2)}{J(\hat{D}, \hat{k}_1, \hat{k}_2)}. \quad (27)$$

Because of Eq. 23, it is possible to store the optimal value of the cost functional obtained from the one-parameter fit with the recovery function $F_1(\cdot;D)$ and use it in calculating the statistic from Eq. 27. Under certain assumptions on the noise process, the cost functional, and the parameter space, if H_0 holds true, it is proved in Banks and Fitzpatrick ((20), their Theorem 4.6)) that the random variable U converges in distribution to a χ-square distributed random variable with one degree of freedom, as the number n of data points goes to infinity. We stress that the assumption on the noise process is only that it is a sequence of independent, identically distributed random variables with mean 0 and finite variance ((20), their Assumption A1).

Here we give a representative calculation to show how this method is applied to our actual data. In the fluorescence recovery experiment for p53-GFP shown in Fig. 6, the optimal residual with the one-parameter model is $J(\tilde{D}, 0, \cdot) = 0.11277$, whereas the optimal residual with the three-parameter model is $J(\hat{D}, \hat{k}_1, \hat{k}_2) = 0.00945$. This gives a value $U = 10.9350$ for the statistic from Eq. 27. The χ-square distribution is $Q(U|1) = 0.00094$, indicating that the null-hypothesis $k_1 = 0$ can be rejected with a very low probability of an erroneous decision. The number of data points $n = 230$ we take as large enough to justify the use of the asymptotic (as $n \to \infty$) result ((20), their Theorem 4.6).

The procedure for detection of outliers is as follows. Let $\{X_1,\ldots,X_n\}$ be the data set in question. Let Q_1 and Q_3 be the first and the third quartiles, respectively. The interquartile range is $D_{13} = Q_3 - Q_1$. We consider a value X an outlier, if $X > Q_3 + 2D_{13}$ or $X < Q_1 - 2D_{13}$. This convention is adapted from Weisstein et al. (38), where we have chosen a greater factor (2 instead of 1.5, as suggested by (38)). If one of the three parameter values (D, k_1, or k_2) is identified as an outlier, the corresponding run is discarded and does not enter the averaging process.

Data collection and evaluation of noise

Two regions were defined in each experiment, one covering the fluorescent compartment entirely (ROI) and one outside (ROC) (Fig. 1). The ROC was used to determine the background signal. The fluorescence measurements are photon-counting rates in kHz, given within ± 100 Hz.

We first investigated the influence of the observation laser beam on the fluorescent p53-GFP molecules. The observation laser beam does not cause loss of fluorescence over the timeframe of the experiment (Fig. 10). Here we address a concern voiced in Waharte et al. ((14), their Hypothesis H2). The background signal is low (data not shown).

Next, we considered the reduced and normalized steady-state signal. In the absence of a concentration gradient, the signal should be constant. The perturbations of this constant signal we consider as noise, regardless of their physical origin. The background signal from the region of control was subtracted from the signal from the region of interest and this was normalized to mean 1. We calculate the standard deviation of the noise to be

$$\sigma = 0.01161. \quad (28)$$

We test the hypothesis of normality of the noise. To this end we apply the Kolmogorov-Smirnov test for equality of distributions ((39), their Section 13.5). For a given set of random values $x_1,\ldots,x_N$, define the (empirical) cumulative distribution function

$$S_N(x) = \frac{1}{N}\{x_i : x_i \le x\}.$$

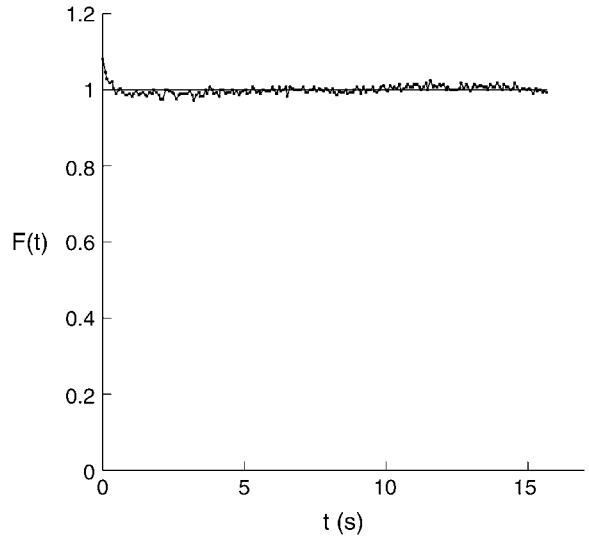

FIGURE 10 The normalized (to mean ''1'') steady-state signal. Photobleaching during observation does not occur. The noise process is stationary.

The Kolmogorov-Smirnov statistic with respect to the hypothesized theoretical probability distribution P is

$$S = \sup_{-\infty < x < \infty} |S_N(x) - P(x)|.$$

The hypothesis of equidistribution is rejected if $K(\sqrt{N}S) \approx 0$, where

$$K(\lambda) = 2\sum_{j=1}^{\infty}(-1)^{j-1}\exp(-2j^2\lambda^2).$$

The value of the Kolmogorov-Smirnov statistics was calculated to be $S = 0.0993$. That gives $K(\sqrt{200}\times 0.0993) = 0.038$. This result prevents us from using the value of the χ-square test to decide about the rejection of a model with full confidence.

Numerical simulation of concurrent bleaching and diffusion

With the help of numerical simulations we tested whether the choice of a piecewise constant initial datum to the recovery process is acceptable. The system equation (Eq. 15) was solved on the spatial domain $(x, t) \in [0, \ell] \times [-0.5, 20]$ for the choices $\kappa = 6.0$ and $D = 6$. The normalized fluorescence intensity profile I is chosen according to Eq. 1 with $c = 10$ and $r = 2.2$. The corresponding (simulated) fluorescence function $\tilde{F}(t)$ was calculated and its asymptotic value $\tilde{F}_\infty$ was used to compute h as indicated in Eqs. 5 and 6, giving $h = 3.37$. The parameter θ was determined to be $\theta = \int_0^\ell \tilde{u}(x, 0)dx = 0.1984$, the simulated bleach depth. The resulting simulated initial datum to the recovery process is shown in Fig. 8.

We then attempted to fit the theoretical recovery function obtained in Eq. 17 to the recovery portion of the simulated fluorescence curve with the choice of θ and h as above (Fig. 9). The so-obtained diffusion constant was $D = 6.5375$, close to the value used in the numerical simulation, $D = 6$.

P.H. thanks Dr. Gustavo Carrero (Department of Mathematics, University of Alberta, Edmonton, Alberta, Canada) and Dr. David Bortz (Department of Mathematics, University of Michigan, Ann Arbor) for pointing out helpful references. He is also grateful to Dr. Erik Boczko (Department of Biomedical Informatics, Vanderbilt University) and Gil Hornung (Weizmann

Institute, Rehovot, Israel) for inspiring discussions. The authors thank Kimberly Drake for carrying out a series of FRAP experiments and Dr. Maria Byrne (Department of Mathematics and Department of Molecular Physiology and Biophysics, Vanderbilt University) for careful reading of the manuscript and valuable comments. And finally, we thank the referees for suggestions that greatly improved the article.

P.H. was supported by National Institutes of Health/NCI grant No. 1-P50-CA113007-02 and by National Institutes of Health grant No. 1-RO1-GM 68953-01. C.E.B. and J.A.P. were supported by National Institutes of Health grants No. CA70856, No. CA105436, No. ES00267, and No. CA68485. E.D. was supported by National Institutes of Health grant No. 1-RO1-GM 68953-01.

REFERENCES

1. Houtsmuller, A. B., and W. Vermeulen. 2001. Macromolecular dynamics in living cell nuclei revealed by fluorescence redistribution after photobleaching. *Histochem. Cell Biol.* 115:13–21.
2. Misteli, T. 2001. Protein dynamics: implications for nuclear architecture and gene expression. *Science.* 291:843–847.
3. Carmo-Fonseca, M., M. Platani, and J. R. Swedlow. 2002. Macromolecular mobility inside the cell nucleus. *Trends Cell Biol.* 12:491–495.
4. Belmont, A. 2003. Dynamics of chromatin, proteins, and bodies within the cell nucleus. *Curr. Opin. Cell Biol.* 15:304–310.
5. Janicki, S. M., and D. L. Spector. 2003. Nuclear choreography: interpretations from living cells. *Curr. Opin. Cell Biol.* 15:149–157.
6. Phair, R. D., and T. Misteli. 2000. High mobility of proteins in the mammalian cell nucleus. *Nature.* 404:604–609.
7. Sprague, B., R. L. Pego, D. A. Stavreva, and J. G. McNally. 2004. Analysis of binding reactions by fluorescence recovery after photobleaching. *Biophys. J.* 86:3473–3495.
8. Phair, R. D., P. Scaffidi, C. Elbi, J. Vecerová, A. Dey, K. Ozato, D. T. Brown, G. Hager, M. Bustin, and T. Misteli. 2004. Global nature of dynamic protein-chromatin interactions in vivo: three-dimensional genome scanning and dynamic interaction networks of chromatin proteins. *Mol. Cell. Biol.* 24:6393–6402.
9. Carrero, G., E. Crawford, M. J. Hendzel, and G. de Vries. 2004. Characterizing fluorescence recovery curves for nuclear proteins undergoing binding events. *Bull. Math. Biol.* 66:1515–1545.
10. Tardy, Y., J. L. McGrath, J. H. Hartwig, and C. F. Dewey. 1995. Interpreting photoactivated fluorescence microscopy measurements of steady-state actin dynamics. *Biophys. J.* 69:1674–1682.
11. Carrero, G., E. Crawford, J. Th'ng, G. de Vries, and M. J. Hendzel. 2003. Quantification of protein-protein and protein-DNA interactions in vivo, using fluorescence recovery after photobleaching. *Methods Enzymol.* 375:415–442.
12. Stewart, Z. A., and J. A. Pietenpol. 2001. p53 Signaling and cell cycle checkpoints. *Chem. Res. Toxicol.* 375:243–263.
13. Weiss, M. 2004. Challenges and artifacts in quantitative photobleaching experiments. *Traffic.* 5:662–671.
14. Waharte, F., C. M. Brown, S. Coscoy, E. Coudrier, and F. Amblard. 2005. A two-photon FRAP analysis of the cytoskeleton dynamics in the microvilli of intestinal cells. *Biophys. J.* 88:1467–1478.
15. Wölcke, J., M. Reimann, M. Klumpp, T. Göhler, E. Kim, and W. Deppert. 2003. Analysis of p53 ''latency'' and ''activation'' by fluorescence correlation spectroscopy. Evidence for different modes of high affinity DNA binding. *J. Biol. Chem.* 278:32587–32595.
16. Flatt, P. M., J. O. Price, A. Shaw, and J. A. Pietenpol. 1998. Differential cell cycle checkpoint response in normal human keratinocytes and fibroblasts. *Cell Growth Differ.* 9:535–543.
17. Goodwin, J. S., K. R. Drake, C. L. Remmert, and A. K. Kenworthy. 2005. Ras diffusion is sensitive to plasma membrane viscosity. *Biophys. J.* 89:1398–1410.
18. Kenworthy, A. K., B. J. Nichols, C. L. Remmert, G. M. Hendrix, M. Kumar, J. Zimmerberg, and J. Lippincott-Schwartz. 2004. Dynamics of putative raft-associated proteins at the cell surface. *J. Cell Biol.* 165:735–746.
19. Phair, R. D., S. A. Gorski, and T. Misteli. 2003. Measurement of dynamic protein binding to chromatin in vivo, using photobleaching microscopy. *Methods Enzymol.* 375:393–414.
20. Banks, H. T., and B. G. Fitzpatrick. 1990. Statistical methods for model comparison in parameter estimation problems for distributed systems. *J. Math. Biol.* 28:501–527.
21. Carrero, G., D. McDonald, E. Crawford, G. de Vries, and M. J. Hendzel. 2003. Using FRAP and mathematical modeling to determine the in vivo kinetics of nuclear proteins. *Methods.* 29:14–28.
22. Braga, J., J. M. P. Desterro, and M. Carmo-Fonseca. 2004. Intracellular macromolecular mobility measured by fluorescence recovery after photobleaching with confocal laser scanning microscopes. *Mol. Biol. Cell.* 15:4749–4760.
23. Stavreva, D. A., and J. G. McNally. 2003. Fluorescence recovery after photobleaching (FRAP) methods for visualizing protein dynamics in living mammalian cell nuclei. *Methods Enzymol.* 375:443–455.
24. Yokoe, H., and T. Meyer. 1996. Spatial dynamics of GFP-tagged proteins investigated by local fluorescence enhancement. *Nat. Biotechnol.* 14:1252–1256.
25. Houtsmuller, A. B., S. Rademakers, A. L. Nigg, D. Hoogstraten, J. H. J. Hoeijmakers, and W. Vermeulen. 1999. Action of DNA repair endonuclease ERCC1/XPF in living cells. *Science.* 284:958–961.
26. Pietenpol, J. A., T. Tokino, S. Thiagalingam, W. S. el-Deiry, K. W. Kinzler, and B. Vogelstein. 1994. Sequence-specific transcriptional activation is essential for growth suppression by p53. *Proc. Natl. Acad. Sci. USA.* 91:1998–2002.
27. Cho, Y., S. Gorina, P. D. Jeffrey, and N. P. Pavletich. 1994. Crystal structure of a p53 tumor suppressor-DNA complex: understanding tumorigenic mutations. *Science.* 265:346–355.
28. Rubbi, C. P., and J. Milner. 2003. p53 is a chromatin accessibility factor for nucleotide excision repair of DNA damage. *EMBO J.* 22:975–986.
29. Allison, S. J., and J. Milner. 2003. Loss of p53 has site-specific effects on histone H3 modification, including serine 10 phosphorylation important for maintenance of ploidy. *Cancer Res.* 63:6674–6679.
30. Allison, S. J., and J. Milner. 2004. Remodelling chromatin on a global scale: a novel protective function of p53. *Carcinogenesis.* 25:1551–1557.
31. Axelrod, D., D. E. Koppel, J. Schlessinger, E. Elson, and W. W. Webb. 1976. Mobility measured by fluorescence photobleaching recovery kinetics. *Biophys. J.* 16:1055–1069.
32. Yang, F., L. G. Moss, and G. N. Phillips. 1996. The molecular structure of green fluorescent protein. *Nat. Biotechnol.* 14:1246–1251.
33. Friedman, P. N., X. B. Chen, J. Bargonetti, and C. Prives. 1993. The p53 protein is an unusually shaped tetramer that binds directly to DNA. *Proc. Natl. Acad. Sci. USA.* 90:3319–3323.
34. Clore, G. M., J. G. Omichinski, K. Sakaguchi, N. Zambrano, H. Sakamoto, E. Appella, and A. M. Gronenborn. 1994. High-resolution structure of the oligomerization domain of p53 by multidimensional NMR. *Science.* 265:386–391.
35. Chène, P. 2001. The role of tetramerization in p53 function. *Oncogene.* 20:2611–2617.
36. Lippincott-Schwartz, J., E. Snapp, and A. K. Kenworthy. 2001. Studying protein dynamics in living cells. *Nat. Rev. Mol. Cell Biol.* 2:444–456.
37. Zauderer, E. 1988. Partial Differential Equations of Applied Mathematics, 2nd Ed. John Wiley & Sons, New York.
38. Weisstein, E. W. 2005. Outlier. From MathWorld—A Wolfram Web Resource. http://mathworld.wolfram.com/Outlier.html.
39. Press, W. H., B. P. Flannery, S. A. Teukolsky, and W. T. Vetterling. 1988. Numerical Recipes in C. Cambridge University Press, Cambridge, MA.